JACS
JOURNAL OF THE AMERICAN CHEMICAL SOCIETY
Communication
pubs.acs.org/JACS

Water-Soluble NIR-Absorbing Rylene Chromophores for Selective Staining of Cellular Organelles

Stefka Kaloyanova,[†,⊥] Yulian Zagranyarski,[‡,⊥] Sandra Ritz,[§] Mária Hanulová,[§] Kaloian Koynov,[†] Andreas Vonderheit,[§] Klaus Müllen,[*,†] and Kalina Peneva[*,†,∥]

[†]Max Planck Institute for Polymer Research, Ackermannweg 10, 55128 Mainz, Germany

[‡]Faculty of Chemistry and Pharmacy, Sofia University 'St. Kliment Ohridski', 1 James Bourchier Ave., Sofia 1164, Bulgaria

[§]Microscopy Core Facility, Institute of Molecular Biology, Ackermannweg 4, 55128 Mainz, Germany

[∥]Laboratory of Organic and Macromolecular Chemistry, Jena Center of Soft Matter, Friedrich Schiller University Jena, Lessingstrasse 8, 07743 Jena, Germany

Supporting Information

ABSTRACT: Biocompatible organic dyes emitting in the near-infrared are highly desirable in fluorescence imaging techniques. Herein we report a synthetic approach for building novel small *peri*-guanidine-fused naphthalene monoimide and perylene monoimide chromophores. The presented structures possess near-infrared absorption and emission, high photostability, and good water solubility. After a fast cellular uptake, they selectively stain mitochondria with a low background in live and fixed cells. They can be additionally modified in a one-step reaction with functional groups for covalent labeling of proteins. The low cytotoxicity allows a long time exposure of live cells to the dyes without the necessity of washing. Successful application in localization super-resolution microscopy was demonstrated in phosphate-buffered saline without any reducing or oxidizing additives.

Fluorescence imaging has emerged as a promising non-invasive, real-time, and high-resolution technique for the detection and visualization of biomolecules and processes in living cells. Among the existing optical imaging methods, fluorescence imaging that uses near-infrared (NIR) light (650–900 nm) has found widespread application both *in vitro* and *in vivo*.[1] The low absorption and autofluorescence from biological structures in this spectral range result in images with reduced background interference, improved tissue penetration depth, and ultimately more precise detection. NIR molecular imaging relies immensely on the design of novel stable and sensitive fluorescent probes. Regardless of the large number of commercially available fluorescent molecules based on organic dyes, fluorescent proteins, or enzyme-mediated tags, there are only a few reporter molecules that cover the NIR region of the spectrum and fulfill the main requirements for biologically suitable probes.[2] Fusion protein expression and enzyme-based recognition processes can ensure efficient and site-selective labeling within cells, but their main limitation is their large size, which can influence the structure and function of the object of interest.[3] Organic dyes have proven to be highly specific and sensitive molecular reporters,[4] and some of them such as Indocyanine green, have been in clinical use for more than 50 years.[5] However, conventional NIR organic chromophores usually suffer from poor hydrophilicity and photostability, low quantum yield, insufficient stability in biological systems, and low detection sensitivity. Dyes active in the NIR region often contain an extended or elongated π-conjugated system, which unfortunately leads to decreased photostability, strong tendency to aggregate in aqueous solution, and poor cell permeability, thus limiting their biological applications.[6] While the chemical modification of the chromophore scaffold of many of the existing NIR dyes, e.g. with water-solubilizing groups, has improved their performance in *in vitro* experiments, it has also revealed new hurdles. Dyes with large molecular weight, apart from being more challenging to synthesize, can interfere with biomolecules and are readily applied *in vivo*. Therefore, great effort has been invested in improving the biocompatibility and the photochemical properties of the existing NIR chromophores. Several examples of NIR-absorbing rylene dyes have been reported, which all possess characteristically exceptional photochemical stability.[7] However, none of these structures described so far can be applied in biological experiments due to their large size, intrinsic hydrophobicity, and lack of functional groups that would allow attachment to biomolecules. Herein, we report the first low-molecular-weight, NIR-absorbing members of the rylene family, which are soluble in aqueous environments and contain a *peri*-fused guanidine. The facile preparation of both the naphthalene and perylene monoimide chromophores allowed us to also attach triphenylphosphine groups that facilitated efficient targeting of subcellular structures or functional groups that permitted covalent labeling of proteins and nucleic acids. Fluorescence microscopy imaging in living and fixed cells stained with the guanidine-functionalized rylenes demonstrated their efficient mitochondrial targeting and excellent biocompatibility. Ground-state depletion followed by individual molecular return (GSDIM) revealed stable "bright dark-state switching" of the perylene monoimide dye, selective for mitochondria, in phosphate buffer saline (PBS) without any supplements, thus demonstrating its application in super-resolution microscopy (nanoscopy).[1a,8]

Received: October 5, 2015
Published: February 18, 2016

DOI: 10.1021/jacs.5b10425
J. Am. Chem. Soc. 2016, 138, 2881–2884

The synthesis of the naphthalene dyes starts from 4,5-dibromo-1,8-naphthalic anhydride (**1**), which was prepared as described previously[9] (SI, Scheme S1). After imidization of **1** with 6-amino-1-hexanol, the *N*-(6-hydroxyhexyl)-guanidine derivative (**2a**) was obtained by a substitution reaction of **2** with guanidine. The conversion of **2a** in the presence of phosphorus tribromide furnished compound **3**, which was applied further in the preparation of the functional derivatives **4** and **5**.

The higher homologue perylene monoimide was synthesized starting from the 9,10-dibromo-functionalized perylene monoanhydride **6** via a Hunsdiecker reaction as described before.[10] Following the same synthetic approach applied for the naphthalene chromophore, brominated perylene monoimide derivative **8** was prepared (Scheme 1) and used as staring

Scheme 1. Synthesis of Perylene Monoimide Dyes 9 and 10[a]

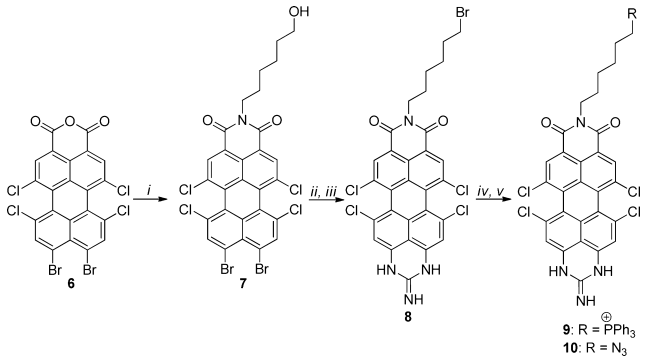

[a](i) 6-amino-1-hexanol, NMP/AcOH, 105 °C, 2 h, 42%; (ii) guanidine hydrochloride, K_2CO_3, DMF, 110 °C, 40 min, 50%; (iii) PBr_3, ethyl acetate, 70 °C, 3 h, 70%; (iv) in case R = P^+Ph_3, PPh_3, 1,2-dichlorobenzene, MW 300 W, 160 °C, 6 h, 35%; (v) when R = N_3, NaN_3, DMF, rt, 24 h, 81%.

material for the synthesis of **9** and **10**. We thus obtained perylene-based NIR chromophores in a single step through the introduction of a guanidine substituent at the so-called *peri*-positions of the rylene scaffold. Furthermore, the synthesized monofunctional dyes are small molecules with excellent solubility in aqueous solutions (1.37×10^{-3} mol/L for **4** and 5.28×10^{-4} mol/L for **9**).[11] They demonstrate a large bathochromic shift in both their absorbance and emission properties (Table 1, compounds **9** and **10**) compared with other water-soluble perylene[12] and terrylene diimide[13,14] fluorophores. Additionally the photophysical characteristics of compounds **4**, **5**, **9**, and **10** show their high molar absorptivity and quantum yield (Table 1). All naphthalene monoimide (NMI) compounds have very narrow absorption and emission maxima, which is a very valuable feature for multicolor staining protocols where a combination of different dyes is often applied.

We then incorporated a triphenylphosphine (TPP) moiety at the imide, combining the selectivity of TPP toward mitochondria with the excellent photochemical properties of the rylene dyes (compounds **4** and **9**). Mitochondria are universal targets in all cancer cells, and new information about functional and structural differences between healthy and malignant cells is currently emerging.[15] Visualizing mitochondria by fluorescent dyes can provide important information about these organelles and their key function in many cellular processes, like apoptosis. However, most of the conventional fluorescence labels for mitochondria are easily released during fixation, and their retention depends on

Table 1. Compounds 4, 5, 9, and 10 and $\lambda_{max}/\lambda_{em}$, ε, and Φ_f Values

compound	$\lambda_{max}/\lambda_{em}$ [nm]	ε [$M^{-1}\cdot cm^{-1}$]	Φ_f
4	458/466[a]	41 000[a]	0.59[d]
	461/467[b]	21 460[b]	0.22[e]
5	458/467[a]	58 200[a]	0.60[d]
	459/468[b]	16 860[b]	0.21[e]
9	709/725[c]	79 590[c]	0.38[d]
	721/730[b]	31 320[b]	0.11[e]
10	708/723[c]	83 230[c]	0.25[c]
	645/731[b]	18 340[b]	0.10[e]

[a]ε measured in methanol solution at room temperature. [b]ε measured in Tris buffer solution. [c]ε measured in dimethyl sulfoxide solution at room temperature. [d]Φ_f of compounds **4** and **5** measured in ethanol using Acridine Yellow (Φ_f = 0.47) as standard, Φ_f of compounds **9** and **10** determined using Rhodamine 800 (Φ_f = 0.25)[10] in ethanol as standard. [e]Φ_f of compounds **4** and **5** measured in aqueous buffer using Acridine Yellow (Φ_f = 0.47) as standard, Φ_f of compounds **9** and **10** determined using Rhodamine 800 (Φ_f = 0.25) in aqueous buffer as standard.

membrane potential. Furthermore, selectivity decreases with increased concentration and usually co-staining of the endoplasmic reticulum also occurs.[16] Recently, the selective localization of low-molecular-weight drugs bearing TPP groups in the mitochondria was reported.[17]

The cellular uptake and the staining ability of NMI and PMI chromophores **4** and **9** were investigated by fluorescence microscopy on different cell lines: African green monkey kidney cells (Vero B4), human cervical carcinoma cells (HeLa), human osteoblastoma cells (U-2 OS), and breast cancer cells (MCF7), resulting in bright fluorescence and fast cellular internalization after a short incubation time (5−10 min). Compounds **4** and **9** were compared with the nonfunctionalized naphthalene dye (2-imino-7-octyl-2,3-dihydropyrido[3,4,5-*g*,*h*]perimidine-6,8-(1*H*,7*H*)-dione **12**, Scheme S3), which stained the endoplasmic reticulum at low concentrations, while the nonfunctionalized perylene dye **14** (Scheme S4) showed a weaker cell staining and was concentrated primarily in vesicular structures (Figure 1A).

Both dyes **4** and **9** selectively localized in the mitochondria in all tested cell lines (Figure 1B). The mitochondria staining of **4** and **9** in living Vero-B4 cells co-localized with the commercial mitochondrion-selective MitoTracker Green FM dye (Figure 1C). Fast accumulation of the dyes in the cellular interior was observed after 5−10 min.

After 15−20 min a selective staining with low background appeared for **9** (2.5−5 μM), even in cells without washing (Figure S9). During the measurements, the cells did not exhibit any structural changes, indicating good biocompatibility and no toxicity. The staining with **9** was mainly preserved in fixed Vero-B4 and U-2 OS cells (Figure S10). Both **4** and **9** showed good photostability and allowed prolonged fluorescence imaging without significant photobleaching (Figure S11).

The cell viability was assessed by detecting the ATP amount, which is closely related to the mitochondrial activity (Cell Titer Glo, Promega). Different incubation conditions were used in order to determine the direct effect of the dyes after 1, 1.5, and 24 h and to simulate the duration of a typical staining experiment. Comparison with commercial MitoTracker Green FM and MitoTracker Deep Red was also performed (Figure S12). In all cases the cell viability surpassed 80−90% at concentrations below 10 μM (Figure S12, Table S1). Thus, allows efficient staining of

DOI: 10.1021/jacs.5b10425
J. Am. Chem. Soc. 2016, 138, 2881−2884

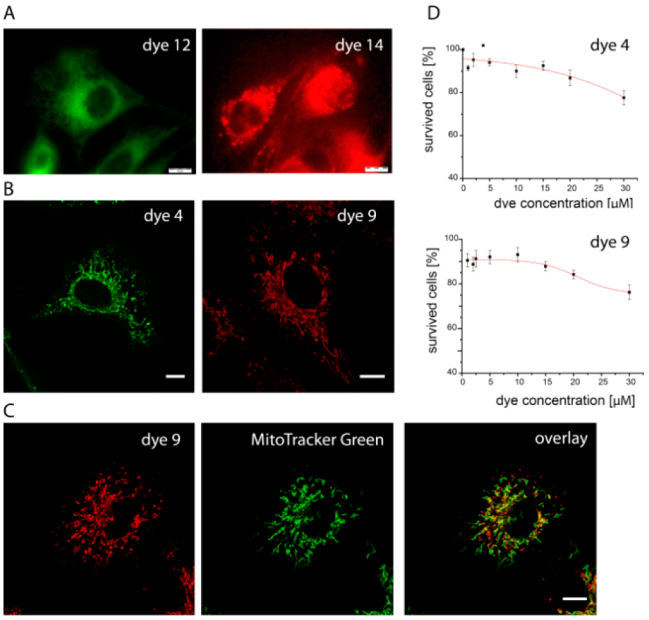

Figure 1. Live cell staining and viability curves of the triphenylphosphine functionalized dyes. (A) Fluorescence widefield images of living HeLa cells stained with **12** (green pseudocolor, 1 μM, 60 min) and **14** (red pseudocolor, 1 μM, 60 min) before functionalization. (B) Respective dyes **4** (green pseudocolor, 20 μM, 20 min) and **9** imaged by confocal laser scanning microscopy after functionalization with TPP. (C) Double staining of mitochondria in VeroB4 cells with **4** (red pseudocolor, 2.5 μM, 20 min) and MitoTracker Green FM (green pseudocolor, 200 nM, 20 min) confirmed the mitochondria staining by the colocalized structures (yellow). (D) Viability test (CellTiter-Glo) of MCF-7 cells treated for 1.5 h with increasing concentrations of **4** or **5**. Survived cells (%) normalized to untreated control cells. Mean value and standard deviation calculated from three replicates. Scale bars 10 μm.

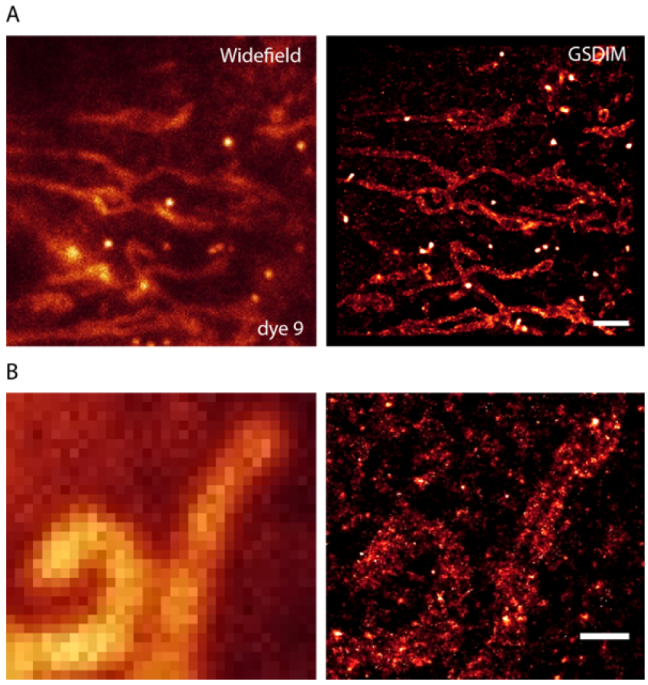

Figure 2. Comparison of wide-field (left) and super-resolved images (right) of mitochondria in fixed VeroB4 cells stained with **9** (5 μM, 20 min). Cells were fixed with 4% paraformaldehyde and immersed in DPBS (pH 7.4) for imaging. Wide-field images have a size of 18 × 18 μm (180 × 180 pixels). Super-resolution images were reconstructed from 30 000 single frames (10 ms exposure) in the wide-field mode (A) or TIRF (total internal reflection) mode (B). Scale bars 2 μm (A) and 500 nm (B).

mitochondria in live cells as well as repetitive microscopy observations at different times.

The diameter of mitochondria is close to the resolution limit of conventional light microscopy between 250 and 500 nm, which makes it challenging to observe submitochondrial structures. Recently, striking insights into architecture and function of submitochondrial structures like the outer and inner membrane proteins or nucleoids could be achieved by super-resolution microscopy.[1a,8] We therefore tested the superresolution potential of **9** by the single-molecule imaging technique GSDIM microscopy.[18] In this method, reducing and oxidizing additives and the removal of oxygen stabilize the transient off-states necessary for the photoswitching process. We investigated the performance of compound **9** in fixed VeroB4 cells and several buffer systems commonly used in super-resolution microscopy: PBS, PBS supplemented with the reducing agent MEA (β-mercaptoethylamine, 1 mM or 10 mM), or an oxygen removal buffer (Glox: glucose oxidase, catalase). Figure 2A,B shows examples of super-resolution images of mitochondria stained with **9** in fixed VeroB4 cells imaged in PBS. The dye molecules were localized with 20.8 nm localization precision (σ) corresponding to a theoretical optical resolution of 49 nm resolution (FWHM = 2.35 * σ) (Figure S13). Generally, it was possible to increase the number of blinking events by activation with a 405 nm laser (Figure S14). Interestingly, good photoswitching behavior for imaging of mitochondria was obtained in PBS. The addition of MEA (1 mM/10 mM) did not significantly improve the imaging quality or resolution. The photoswitching behavior of **9** in PBS buffer could be due to the intrinsic redox potential of the mitochondria[19] and offers the potential to apply **9** in live-cell super-resolution imaging.

In order to compare the photostability of the perylene chromophores reported here with fluorophores commonly used in the field of nanoscopy, single-molecule fluorescence measurements of proteins labeled with the following dyes Alexa647, Atto647N, Cage635, and **10** were performed in total internal reflection geometry. In order to determine their intrinsic stability and switching behavior, the mean photon intensity and localization precision of the four fluorophores were measured in PBS (Figure S7). Although all dyes bleached relatively fast in PBS, repeated blinking events were observed for **10** and Cage635, in contrast to Alexa647, which showed mostly one single event before photobleaching (Figure S7C). In Glox buffer, **10** and Atto647N showed the highest stability, expressed as 90% surviving events, followed by Cage (65%) and Alexa647 (12%) (Figure S8C). Independent from the buffer system that was applied, all chromophores showed similar mean photon intensities and lateral localization precision (σ) of 20 nm.

To acquire additional data for the photostability of the novel chromophores not only in adsorbed state but also in solution, fluorescence correlation spectroscopy[20] was performed in buffer solution (see SI for details). Compounds **4** and **9** were compared with Rhodamine 123 at different excitation laser powers (Figure S15). Rhodamine 123 is often used for labeling mitochondria in live cells and shows intrinsic fluorescence prior to binding to biological objects in comparison with MitoTracker Deep Red, which is nonfluorescent in solution. The solution of compound **4** did not reveal any changes in fluorescence intensity in the range commonly used in FCS experiments (laser powers of up to 30

DOI: 10.1021/jacs.5b10425
J. Am. Chem. Soc. 2016, 138, 2881−2884

μW). For compound **9** even better photostability, similar to that of the Rhodamine 123, was observed in the entire range of laser powers.

Additionally, an azide function was introduced at position 6 in the alkyl chain of both NMI and PMI derivatives **3** and **8**, to investigate the potential of the newly prepared chromophores for covalent labeling of proteins or nucleic acids. Azides efficiently take part in the copper-catalyzed azide−alkyne cycloaddition reaction, which has achieved a widespread implementation in bioorthogonal chemistry. The available amine groups of bovine serum albumin (BSA) were functionalized with propagyl-NHS ester and the terminal ethinyl moieties were coupled with the complementary azide derivative **5**.

Analyzing the conjugate by sodium dodecyl sulfate polyacrylamide gel electrophoresis (SDS-PAGE) gave protein bands that proved the successful labeling of the modified BSA (Figure S16A) with the azide functionalized naphthalene dye **5.**

In summary, our synthetic approach allows preparation of naphthalene monoimides or perylene monoimides with small size, absorption, and emission maxima beyond 700 nm in case of perylene structures. The chromophores possess excellent water solubility, high extinction coefficients, and quantum yields. Furthermore, second functional groups can be introduced for covalent labeling of biomolecules or selective staining of particular cellular compartments like mitochondria or the endoplasmatic reticulum. The novel class of fluorophores presented here can be applied in trafficking studies of tagged polymeric or nanocarriers and thus can stimulate nanomedical research both *in vitro* and *in vivo*.

■ ASSOCIATED CONTENT

Supporting Information

The Supporting Information is available free of charge on the ACS Publications website at DOI: 10.1021/jacs.5b10425.

Figures S1−S16 and Table S1 (PDF)

■ AUTHOR INFORMATION

Corresponding Authors

*kalina.peneva@uni-jena.de

*muellen@mpip-mainz.mpg.de

Author Contributions

⊥These authors contributed equally.

Notes

The authors declare no competing financial interest.

■ ACKNOWLEDGMENTS

The authors are grateful to the International Research Training Group 1404 'Self-organized Materials for Optoelectronics' (DFG) for the financial support. The authors thank Aleksander Szczurek, Kirti Prakash, and Udo Birk for the enlightened discussions about single-molecule localization analysis. Y.Z. is grateful to the Sofia University Scientific Fund (grant 77/2015).

■ REFERENCES

(1) (a) Alander, J. T.; Kaartinen, I.; Laakso, A.; Patila, T.; Spillmann, T.; Tuchin, V. V.; Venermo, M.; Valisuo, P. *Int. J. Biomed. Imaging* **2012**, *2012*, 940585. (b) Folling, J.; Bossi, M.; Bock, H.; Medda, R.; Wurm, C. A.; Hein, B.; Jakobs, S.; Eggeling, C.; Hell, S. W. *Nat. Methods* **2008**, *5*, 943. (c) Heilemann, M.; van de Linde, S.; Schuttpelz, M.; Kasper, R.; Seefeldt, B.; Mukherjee, A.; Tinnefeld, P.; Sauer, M. *Angew. Chem., Int. Ed.* **2008**, *47*, 6172.

(2) (a) Kolmakov, K.; Belov, V. N.; Bierwagen, J.; Ringemann, C.; Muller, V.; Eggeling, C.; Hell, S. W. *Chem. - Eur. J.* **2010**, *16*, 158. (b) Zhang, X.; Bloch, S.; Akers, W.; Achilefu, S. *Curr. Protoc. Cytom.* **2012**, *12*, 12.27.1.

(3) Sun, Y.-Q.; Liu, J.; Lv, X.; Liu, Y.; Zhao, Y.; Guo, W. *Angew. Chem., Int. Ed.* **2012**, *51*, 7634.

(4) Crivat, G.; Taraska, J. W. *Trends Biotechnol.* **2012**, *30*, 8.

(5) Lukinavicius, G.; Umezawa, K.; Olivier, N.; Honigmann, A.; Yang, G.; Plass, T.; Mueller, V.; Reymond, L.; Correa, I. R., Jr.; Luo, Z. G.; Schultz, C.; Lemke, E. A.; Heppenstall, P.; Eggeling, C.; Manley, S.; Johnsson, K. *Nat. Chem.* **2013**, *5*, 132.

(6) Berlier, J. E.; Rothe, A.; Buller, G.; Bradford, J.; Gray, D. R.; Filanoski, B. J.; Telford, W. G.; Yue, S.; Liu, J. X.; Cheung, C. Y.; Chang, W.; Hirsch, J. D.; Beechem, J. M.; Haugland, R. P.; Haugland, R. P. *J. Histochem. Cytochem.* **2003**, *51*, 1699.

(7) (a) Rodriguez-Hernandez, J.; Qu, J. Q.; Reuther, E.; Klok, H. A.; Mullen, K. *Polym. Bull.* **2004**, *52*, 57. (b) Peneva, K.; Mihov, G.; Nolde, F.; Rocha, S.; Hotta, J.-i.; Braeckmans, K.; Hofkens, J.; Uji-i, H.; Herrmann, A.; Muellen, K. *Angew. Chem., Int. Ed.* **2008**, *47*, 3372. (c) Weil, T.; Vosch, T.; Hofkens, J.; Peneva, K.; Mullen, K. *Angew. Chem., Int. Ed.* **2010**, *49*, 9068. (d) Gorl, D.; Zhang, X.; Wurthner, F. *Angew. Chem., Int. Ed.* **2012**, *51*, 6328. (e) Zeng, Z. B.; Lee, S. S.; Zafra, J. L.; Ishida, M.; Zhu, X. J.; Sun, Z.; Ni, Y.; Webster, R. D.; Li, R. W.; Navarrete, J. T. L.; Chi, C. Y.; Ding, J.; Casado, J.; Kim, D.; Wu, J. S. *Angew. Chem., Int. Ed.* **2013**, *52*, 8561. (f) Heek, T.; Wurthner, F.; Haag, R. *Chem. - Eur. J.* **2013**, *19*, 10911. (g) Heek, T.; Nikolaus, J.; Schwarzer, R.; Fasting, C.; Welker, P.; Licha, K.; Herrmann, A.; Haag, R. *Bioconjugate Chem.* **2013**, *24*, 153. (h) Heek, T.; Fasting, C.; Rest, C.; Zhang, X.; Wurthner, F.; Haag, R. *Chem. Commun.* **2010**, *46*, 1884.

(8) Jakobs, S.; Wurm, C. A. *Curr. Opin. Chem. Biol.* **2014**, *20*, 9.

(9) Zagranyarski, Y.; Chen, L.; Jansch, D.; Gessner, T.; Li, C.; Mullen, K. *Org. Lett.* **2014**, *16*, 2814.

(10) Alessi, A.; Salvalaggio, M.; Ruzzon, G. *J. Lumin.* **2013**, *134*, 385.

(11) Prakash, K.; Raju, P. N.; Kumari, K. S.; Narasu, M. L. *E-J. Chem.* **2008**, *5*, 1159.

(12) Feng, J.; Liang, B.; Wang, D.; Xue, L.; Li, X. *Org. Lett.* **2008**, *10*, 4437.

(13) Jung, C.; Muller, B. K.; Lamb, D. C.; Nolde, F.; Mullen, K.; Brauchle, C. *J. Am. Chem. Soc.* **2006**, *128*, 5283.

(14) Zagranyarski, Y.; Chen, L.; Zhao, Y. F.; Wonneberger, H.; Li, C.; Mullen, K. *Org. Lett.* **2012**, *14*, 5444.

(15) (a) Frezza, C.; Gottlieb, E. *Semin. Cancer Biol.* **2009**, *19*, 4. (b) Biasutto, L.; Dong, L. F.; Zoratti, M.; Neuzil, J. *Mitochondrion* **2010**, *10*, 670. (c) Gogvadze, V.; Orrenius, S.; Zhivotovsky, B. *Trends Cell Biol.* **2008**, *18*, 165.

(16) Terasaki, M.; Reese, T. S. *J. Cell Sci.* **1992**, *101*, 315.

(17) (a) Leung, C. W. T.; Hong, Y. N.; Chen, S. J.; Zhao, E. G.; Lam, J. W. Y.; Tang, B. Z. *J. Am. Chem. Soc.* **2013**, *135*, 62. (b) Yang, W. G.; Chan, P. S.; Chan, M. S.; Li, K. F.; Lo, P. K.; Mak, N. K.; Cheah, K. W.; Wong, M. S. *Chem. Commun.* **2013**, *49*, 3428. (c) Lee, M. H.; Park, N.; Yi, C.; Han, J. H.; Hong, J. H.; Kim, K. P.; Kang, D. H.; Sessler, J. L.; Kang, C.; Kim, J. S. *J. Am. Chem. Soc.* **2014**, *136*, 14136.

(18) (a) Lalkens, B.; Testa, I.; Willig, K. I.; Hell, S. W. *Microsc. Res. Tech.* **2012**, *75*, 1. (b) Oddone, A.; Vilanova, I. V.; Tam, J.; Lakadamyali, M. *Microsc. Res. Tech.* **2014**, *77*, 502.

(19) van de Linde, S.; Heilemann, M.; Sauer, M. *Annu. Rev. Phys. Chem.* **2012**, *63*, 519.

(20) (a) Koynov, K.; Butt, H. J. *Curr. Opin. Colloid Interface Sci.* **2012**, *17*, 377. (b) Hinkeldey, B.; Schmitt, A.; Jung, G. *ChemPhysChem* **2008**, *9*, 2019. (c) Veettil, S.; Budisa, N.; Jung, G. *Biophys. Chem.* **2008**, *136*, 38.

DOI: 10.1021/jacs.5b10425
J. Am. Chem. Soc. 2016, 138, 2881−2884